ASI

Carbon – Science and Technology

ISSN 0974 – 0546

http://www.applied-science-innovations.com

RESEARCH ARTICLE Received:28/12/2015, Accepted:30/12/2015

Functionalization and formation of drinking water filter rod from lignite with zeolite, bentonite, and clay

Sumrit Mopoung*, Nimit Sriprang, Jutatip Namahoot, Nantaka Pumfang, Lalita Chuayudom, Weerada Rattanprasit, Siriwan Di-inkaew, Khatriya Jannachai, Dusadeeporn Polkanyim, Rosjaras Bunpum

Department of Chemistry, Faculty of Science, Naresuan University, Phitsanulok, Thailand.

Abstract: A drinking water filter rod was functionalized and formed from a starting mixture of lignite, zeolite, bentonite, and clay. The formation of the filter was studied focusing on the effects of zeolite dosage and sintering temperature in a reducing atmosphere. The sintered filters were characterized by XRD, FTIR, and SEM-EDS. The physical and chemical properties of filters were measured. The results showed that the firing shrinkage, the total shrinkage and hardness increased with increasing sintering temperature. However, mass yield and fixed carbon decreased with increasing sintering temperature. The functional surface groups of the sintered filter exhibited a high content of aluminosilicates and carbon, which were derived from all starting materials. The macropores of sintered filter had dimensions of the channels between particles in the range of 0.2-2 μm.

Keywords: Drinking water filter, functionalization, forming, zeolite, lignite

1. Introduction: The capability to functionalize the interior channels and/or internal surface areas of porous inorganic solids with specific organic or inorganic moieties has dramatically expanded the potential applications in catalysis, separations, optical and optoelectronic devices, drug delivery, sensors, and energy conversion [1]. Clay materials or aluminosilicates have been used as adsorbents, water softeners, catalysts, and mechanical and thermal reinforcement materials. They are used for these purposes due to their high surface area, excellent thermal/hydrothermal stability, high shape selectivity, and superior ion-exchange ability. They have also been used as polymer fillers, which allowed to expand their application range to innovative areas such as medical and biological fields as well as sensors, filtration membranes, energy storage materials, and novel catalysts [2]. These materials possess a layered structure and are considered to act as host materials. The adsorption capabilities of these materials result from the net negative charge on the structure of the minerals, which give clay the ability to adsorb positively charged species. Their adsorption properties are also related to their high surface-area and high porosity. There has been an increasing interest in utilizing clay minerals such as bentonite, kaolinite, and diatomite for their capacity to adsorb both inorganic and organic molecules [3]. In addition, the plastic property of clay is appropriate for processing through extrusion. Furthermore, after appropriate subsequent drying and heating treatments, these clay based materials become rigid solids with good physico-chemical properties [4]. The natural zeolite has high cation-exchange capacity and exhibits high adsorption capacity for methylene blue, rhodamine B [5], and heavy metals [6]. However, it has a negligible adsorption capacity for organic contaminants from aqueous solution [6]. Zeolites are hydrated aluminium-silicate minerals in which the aluminium and silicon polyhedra are linked by the sharing of oxygen atoms [7]. They are highly porous

aluminosilicates with different cavity structures. Their structures consist of a three dimensional framework, having a negatively charged lattice. The negative charge is balanced by cations which are exchangeable with certain cations in solutions [3]. Bentonite is another natural clay, which contains mainly the smectite and kaolinite mineral phases. Smectite is a fairly expanding three sheet phyllosilicate, where the tetrahedral $[SiO_4]^{4-}$ to octahedral $[AlO_3(OH)_3]^{6-}$ ratio is 2:1 and the charge of the three-sheet layer is 0.5–1.2 e/unit cell (negative charge). This charge arises from the isomorphous substitution of Al^{3+} and Si^{4+} in the tetrahedral sheet and Mg^{2+} for Al^{3+} in the octahedral sheet. This group possesses no hydroxyl functionality within the interlayer. However, kaolinite and serpentine are two-sheet phyllosilicates, where the tetrahedral $[SiO_4]^{4-}$ per octahedral $[AlO_3(OH)_3]^{6-}$ ratio is 1:1 and the charge of the two-sheet layer is 0 *e*/unit cell. Since bentonite contains dominantly the smectite mineral having permanent negative charge, which is usually compensated by the exchangeable cations present within the interlayer space. Therefore, bentonite clay shows fairly high cation exchange capacity and good water swelling properties [8]. These natural inorganic materials have potential for surface functionalization. For example, hybrid inorganic/organic adsorbents have been synthesized using mixtures of diatomite and carbon charcoal as precursors, which are used for the removal of *p*-cresol from aqueous solution [9]. Montmorillonite clay has been used to prepare carbon/clay nanocomposites and composites by calcination in a reducing atmosphere. It is high carbon content which capacities adsorption of methylene blue and gasoline [10]. The adsorbent, which contains 45.94 % zeolite, 15.31 % limestone, 4.38 % activated carbon, and rice husk carbon respectively, and 30 % of ordinary Portland cement (as a binder), has been used for adsorption of chemical oxygen demand and ammoniacal nitrogen causing contaminants in landfill leachate treatment. A combination of activated carbon and zeolite, as a natural ion exchanger, in composite media provides both hydrophobic and hydrophilic surfaces for the removal organic and inorganic (especially ammonia) contaminants [11]. In this composite, the carbon is essential to preserve the mesoporous structure of the source. Furthermore, the addition of aluminum on mesoporous silica is critical for the stability of the zeolitic building units on the surface of mesopores [12]. The granular X-type zeolite/activated carbon composites have been prepared from elutrilithe by adding pitch powder and solid SiO_2. The composites had a hierarchical pore structure and a high content of carbon in the composites [13]. The adsorption capacity of carbon-zeolite composites depends on carbon content. For example, the adsorption of phenol on carbon and natural zeolite composite is increased with increasing carbon content of the composite [6]. The composite prepared by liquid phase impregnation of zeolite templates using lignin solutions as carbon precursor have high microporosity and mesoporosity. The templated carbon present surface chemistry with a relatively high amount of nitrogen and oxygen stable surface groups, such as pyrrolic, pyridinic, hydroxyl and carbonyl, which were formed by transfer of ammonia and oxygen from the surface of the zeolite template to the carbon materials during the synthesis [14]. Composite material consisting of activated carbon and zeolites has successfully been prepared using coal fly ash, which contains SiO_2, Al_2O_3, and unburned carbon. It was activated by NaOH fusion treatment at 750 ºC in a N_2 atmosphere for conversion into zeolites Na–X and/or Na–A with good crystallinity by hydrothermal treatment [15]. Silica/activated carbon (2:3) composite with high efficiency in the removal of nickel ions has also been prepared [16]. These composites were used for many purposes. For example a composite adsorbent synthesized from activated carbon, silica-gel, and $CaCl_2$ has been used for adsorption cooling and dehumidification systems [17]. A composite prepared from melamine-modified phenol–formaldehyde resins via steam activation at different activation temperatures (700–950 ºC) was used for CO_2 capture at atmospheric pressure [18]. Solid sorbents derived from mixtures of montmorillonite, activated carbon, and cement have also been used for sorption of phenol and 4-nitrophenol [19].

The aim of this research was to study the effects of zeolite dosage and sintering temperatures on

the formation and functionalization of water filters using the addition of bentonite and local clay as binder. The composition of the filter and presence of functional groups after sintering was investigated by Fourier transform infrared spectrometry, X-ray diffraction, and scanning electron microscopy equipped with energy dispersive spectrometer.

2. Materials and methods

2.1 Preparation of materials: Zeolite (commercial grade), bentonite (commercial grade), local clay (obtained from Tambol Tapoh, Muang District, Phitsanulok Province, Thailand), and lignite (obtained from the Mae Moh Basin, Lampang Province, Thailand) were ground and sieved (Laboratory test sieve, Retsch, Germany) to 200 mesh. These materials were mixed to prepare mixtures containing zeolite (5, 10, or 30 wt.%), bentonite (10 wt.%), clay (10 wt.%), and charcoal (60, 90, or 95 wt.%). The mixtures of starting materials were wetted with water (20 % by volume) and borax (5 wt.%, commercial grade) was added. The thermal behavior of the starting mixtures was investigated by differential scanning calorimetry (DSC-1, Mettler). The wetted mixtures were pressed into a PVC pipe (ϕ = 12.7 mm, long = 50 mm). The percent of drying shrinkage, percent of firing shrinkage of the samples were measured by the methods of de Sa et al. [20], and Rasmussen et al. [21], respectively. The percent mass yields of sintered filters were also measured. The wetted samples were dried in an oven (SL shellab, 1350 FX, USA) for 24 h. The dried samples were then placed into a ceramic box and covered with foil, quartz powder, and closed by a lid. The samples were then sintered in an electric furnace (Fisher Scientific Isotemp ® Muffle furnace) under a reducing atmosphere at temperatures of 400 ºC, 500 ºC, 600 ºC, or 700 ºC with 1 h soaking time. Triplicate samples were used for all experiments. The sintered samples were characterized by X-ray powder diffractometer (XRD, PW 3040/60, X' Pert Pro MPD) with a Cu tube anode, a Fourier transform infrared spectrometer (Spectrum GX, Perkin Elmer), and scanning electron microscope equipped with energy dispersive spectrometer (SEM-EDS, LEO 1455 VP).

3. Results and discussion

3.1 Differential scanning colorimeter study: Figure 1 shows the endothermic peak of a representative DSC curve obtained from pyrolysis of mixture of starting materials (45 wt.% lignite, 30 wt.% zeolite, 10 wt.% bentonite, 10 wt.% local clay, and 5 wt.% borax) in pure N_2. The 149.11 ºC peak is attributable to endothermic evaporation of volatile moisture [22]. In general, peaks in the range of 100-150 ºC can be attributed to low-temperature physical desorption of water and gases [23]. The minor peaks at 480 and 550 ºC are attributed to dehydroxylation, which is the removal of hydroxyl groups from Al-OH bonds [22]. These results are in line with the FTIR data (Figure 3d), in which the OH group of sintered filter materials disappeared. It was observed that the degradation of the mixture of starting materials is low, which results in no firing shrinkage of sintered filters obtained at 400 ºC. Mixing with zeolite only or a mixture of zeolite, bentonite, and clay could improve the formation of the mixture of the starting materials by wet method.

Table (1): Percent of drying shrinkage, firing shrinkage, total shrinkage, and mass yield of sample prepared from 45 wt.% lignite, 30 wt.% zeolite, 10 wt.% bentonite, 10 wt.% local clay, and 5 wt.% borax with sintering at 400-600 ºC

Temperature ºC	Percent of drying shrinkage	Percent of firing shrinkage	Percent total of shrinkage	Mass yield (wt.%)	Fixed carbon (wt.%)	Hardness kg/cm^2
110	3.98±0.23	-	-	-	21.26	53.59
400	-	0.00±0.00	3.98±0.12	89.59±0.24	28.39	7.84
500	-	4.01±0.17	7.99±0.20	87.67±0.37	22.32	10.10
600	-	4.35±0.14	8.33±0.19	76.52±0.32	11.66	15.05

This is because the mixing with zeolite and clay considerably affects compressive strength. Bentonite is an inorganic binder capable of improving strength of resulting composite materials [24]. However, these mixtures are forming after sintering at 400-700 ºC. The carbon content of sintered samples obtained with sintering at 700 ºC is also reduced after sintering. In this case, the decomposition of carbon during sintering occurred due to the catalytic effects of zeolite surface and deeper volatilization of the carbon at high temperatures [14].

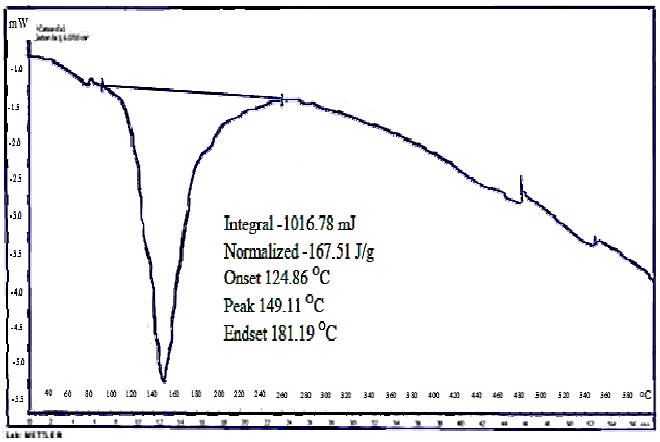

Figure (1): DSC curve of the mixture of starting materials (45 wt.% lignite, 30 wt.% zeolite, 10 wt.% bentonite, 10 wt.% local clay, and 5 wt.% borax).

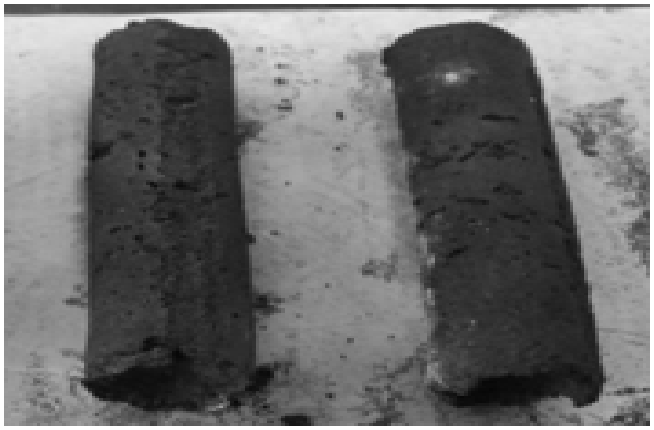

Figure (2): the filter formed from the mixture of starting materials containing 45 wt.% lignite, 30 wt.% zeolite, 10 wt.% bentonite, 10 wt.% local clay, and 5 wt.% borax after sintering at 400 ºC.

On the other hand, the mixtures containing 5 wt.% borax additive could be formable from temperature above 400 ºC, as shown in Figure 2. Since borax is a fluxing reagent [25]. It can be reduced at the sintering temperatures [26] of these mixtures. Salem and Sene [24] have reported that mixtures with high content of zeolite, bentonite, and kaolin could be forming at ≥ 600 ºC. However, the mixtures in this study were mixed with lignite, which is quite volatile at high temperatures. Some carbon content of lignite was volatized after sintering. This effect caused the reduction of strength of sintered samples with formability.

3.2 The percent of drying shrinkage, firing shrinkage and total shrinkage: The percent of drying shrinkage, firing shrinkage, and total shrinkage were determined only for filters prepared from 45 wt.% lignite, 30 wt.% zeolite, 10 wt.% bentonite, 10 wt.% local clay, and 5 wt.% borax at sintering temperature of 400-600 ºC, as shown in Table 1. It was shown that the firing shrinkage increased with the increase in sintering temperature. Consequently the total shrinkage increased with increasing sintering temperature as well. It was observed that the sintered filter prepared at 400 ºC has no firing shrinkage. This may be due to very low degradation of the aluminosilicate compounds at this temperature [27]. The mass yield of the filters decreased with increasing sintering temperature. The mass loss involved dehydroxylation of kaolinite, with the removal of hydroxyl groups from Al-OH bonds [22], and decomposition of lignite, where carbon content was more volatilized as sintering temperature increasing [14]. It was observed that the mass yields of sintered filters are relatively high. This is because zeolite, bentonite, and clay are inorganic materials which are thermally stable [1]. Thus the amount of fixed carbon in sintered filters decreased with increasing sintering temperature, resulting in concomitant decrease of mass yield. It was shown that the mass yield of

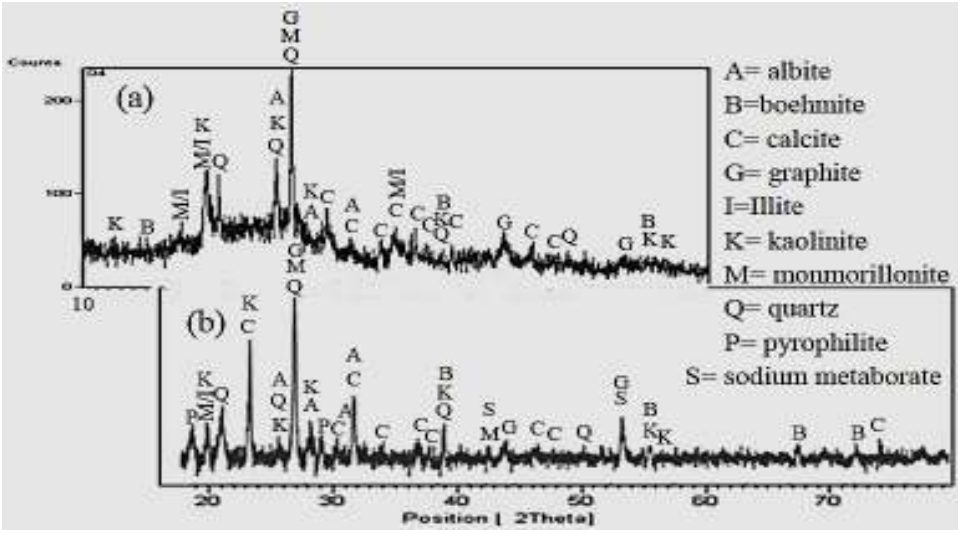

Figure (3): X-ray diffraction patterns of (a) lignite and (b) filter obtained with sintering at 400 ºC.

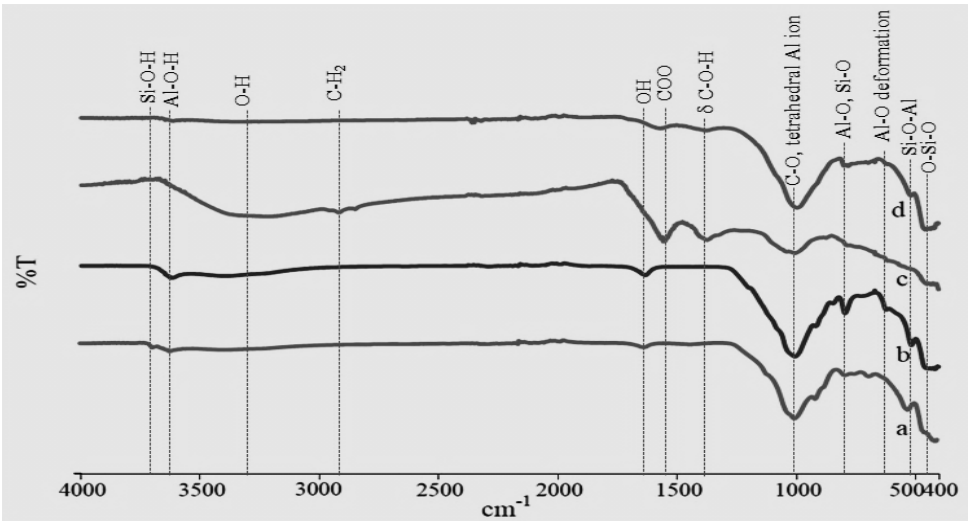

Figure (4): FTIR spectra of (a) zeolite (b) bentonite (c) lignite and (d) filter obtained with sintering at 400 ºC.

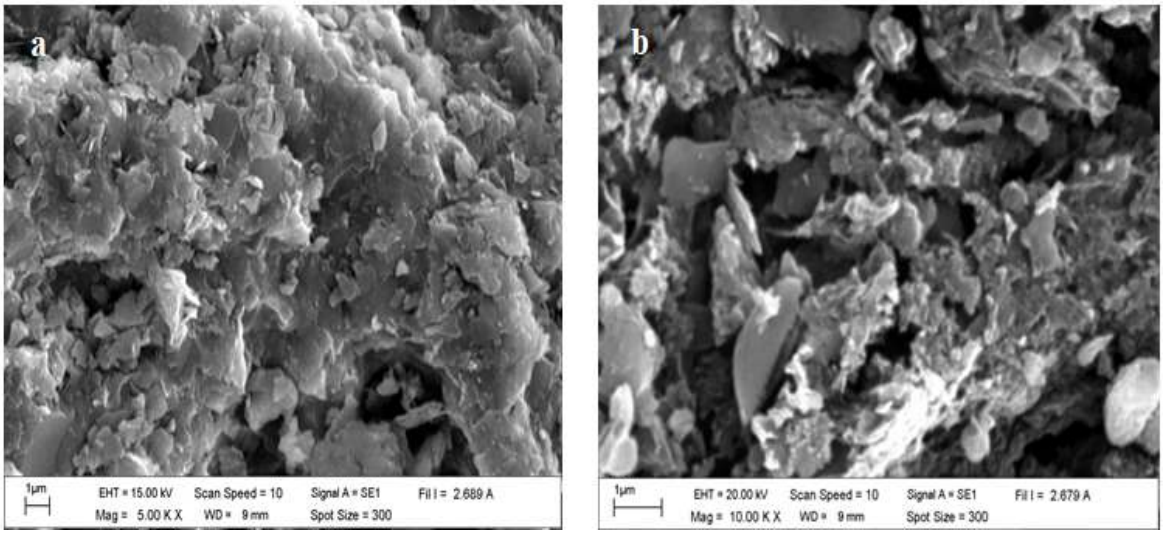

Figure (5): SEM morphology of (a) lignite (b) filter obtained with sintering at 400 ºC.

sintered filters depends on decomposition of carbon content in the mixtures. In addition, it was observe that the fixed carbon content of mixture after drying at 110 °C is relatively low when compared to the sintered filters. This is because of the high content of volatile matter in lignite (69.02 wt.%) [28], which results in lower carbon content.

The hardness of sintered filters increased with increasing sintering temperature. This may be attributed to the decreasing porosity of sintered filters as sintering temperature increases, which is the result of dehydroxylation and decomposition during sintering [29]. This result is directly related with the reduction of carbon content of sintered filter as function of increasing sintering temperature. It could reflect that the sintered filter has higher interfacial strength with good interconnectedness as a result of higher sintering temperature [30]. The hardness of all sintered filters is higher than the limit set by the Thai Industrial Standards Institute (700±10 *k*Pa or 7.1380 kg/cm^2). Sintered filters obtained with sintering at 500-600 ºC have hardness comparable to strong pelletized grey alder wood base activated carbon sintered at 600 °C [31]. However, the hardness of all sintered filters is lower than the hardness of starting lignite. This is due to the release of volatile material from all starting materials at high temperature [32]. Thus, all of the sintered filters are softened.
Due to the results discussed above, the filter obtained by sintering at 400 ºC was used for further characterization as it had lowest shrinkages and a higher standard hardness.

3.3 X-Ray diffraction analysis: Figure 3a shows the X-ray diffractogram of lignite. The background intensity of XRD, seems to be high and exhibits signals of highly disordered materials in the form of amorphous carbon [32] in both lignite and sintered filter. The main mineralogical component of lignite are kaolinite ($Al_2Si_2O_5(OH)_4$), montmorillonite ($Na_{0.33}(Al_{1.67}Mg_{0.33})Si_4O_{10}(OH)_2$), quartz ($SiO_2$), calcite ($CaCO_3$), muscovite ($KAl_2(AlSi_3O_{10})(OH)_2$)/illite ($K_{1.5}Al_4(Si_{6.5}Al_{1.5})O_{20}(OH)_4$), and boehmite (AlO(OH)), which are common in lignite [33]. Peaks of crystalline order of some graphite in lignite have been detected at 26.5º, 44.5º and 53.5º [34]. The peaks in the diffractogram attributed to kaolinite are at 12.5º, 20º, 23.1º, 25.5º, 28.1º, 39º, 55.5º, and 56.9º [22]. Peaks at 27.9º and 42.8º correspond to montmorillonite. Furthermore, peaks corresponding to quartz, can be found at 21º, 26.8º, 36.5º, 39.5º, 50.1º, 52.3º, 55º, 60º, and 68.1º [22]. The peaks of calcite appear at 29.5º, 31.8º, 33.9º, 35º, 37º, 38º, 46.2º, 47.9º, and 74º. The peaks at 18º, 20º, and 35º corresponded to muscovite/illite [22]. Peaks of boehmite were found at 15º, 39º, 55.5º, 67.2º, and 72.1º [33]. Finally, albite is also common component in lignite found at very low concentrations. The peaks of albeit occur at 25.5º, 28.1º, 31º, and 31.9º [33].

After modification with zeolite, bentonite, and clay the sintered filter contained kaolinite, montmorillonite, quartz, calcite, muscovite/illite and boehmite as its components (Figure 3b). Furthermore, pyrophilite is also found in the sintered filter with peaks at 19.2º, 29º, and 35º. These minerals are found in zeolite, bentonite, and clay [24] as well as in lignite [33]. Additional peaks attributed to sodium metaborate ($NaBO_2$) were found 53.46º and 42.30º in the filter [35]. Sodium metaborate was produced from borax ($Na_2B_4O_7$) by chemical reaction with metal oxide [36].

3.4 FTIR analysis: It can be seen from Figure 4 that zeolite and bentonite have almost identical vibrational bands. Since it was shown that the surface functional groups of both are similar, both materials are aluminosilicates [7, 8]. The surface functional groups of the filter (Figure 4d) seem to be the sum of the functional groups of all raw materials (Figure 4a-c). The peak at about 3650 cm^{-1}, which originated from zeolite (Figure 4a) and bentonite (Figure 4b), can be attributed to the AlO-H groups and bridging acidic hydroxyls Si-O(H)-Al. The weak peak at 3750 cm^{-1}, which originated from zeolite (Fig. 4a), can be attributed to SiO-H groups. The broad band found at 3200-3400 cm^{-1}, which belongs to lignite (Figure 4c), and the peak at 1633 cm^{-1}, which belongs to zeolite (Fig. 4a) and bentonite (Figure 4b), disappeared after sintering at 400 ºC. These features are associated with Si-OH stretching and O-H stretching vibrations of adsorbed water

molecules [37]. It was shown that the adsorbed water molecules were removed after sintering at 400 ºC. The very weak peaks found at about 2850 cm^{-1} and 2950 cm^{-1} of lignite, due to C-H_2 stretching [38], disappeared after sintering. The vibration bands appearing around 1010 cm^{-1} and between 800 and 400 cm^{-1} are attributed to the characteristic behavior of aluminosilicate containing materials. The weak peak at around 800 cm^{-1} can be associated with Al–O or Si–O symmetric stretching vibrations. Furthermore, the strong band at about 1010 cm^{-1}, found in all of the materials, was attributed to tetrahedral Al ions [37] or CO [18]. This peak also remained in the filter. The two peaks at 1554 cm^{-1} and 1350 cm^{-1} of lignite were attributed to carboxylates and/or metal-bonded carboxylates [39]. These peaks remained in filter. However, the peak at 1350 cm^{-1} found in the filter may be also due to B–O originating from $Na_2B_4O_7$ [35]. The intensity of these peaks is weakening after sintering. It was shown that some carboxylate groups were removed during sintering. The weak peak at 630 cm^{-1} for bentonite (Figure 4b) was assigned to Al–O deformation [40]. This peak remained in the filter after sintering. The vibration bands of Si–O–Al (540 cm^{-1}) in tetrahedral and octahedral sheets of kaolinite, and O–Si–O (480 cm^{-1}) [37] from zeolite and bentonite were found in the sintered filter. These functional groups are expected to contribute to ion-exchange processes as well as adsorption process for the removal of heavy metal cations [41].

3.5 SEM analysis: Figure 5 shows the SEM micrographs of lignite (Figure 5a) and sintered filter obtained with sintering at 400 ºC (Figure 5b). Lignite has open porous, rough surface and quite dense texture supporting its high hardness (Table 1). The sintered filter has channels as well as a rough surface. The channel size between particles is in the range of 0.2 to 2 μm (Figure 5b). The channels and surface of lignite particles appear dispersed in between the clay or aluminosilicate mineral with a heterogeneous distribution. It was observed that the sintered filter has higher porosity and lower density than lignite. This was attributed to the reduction of elemental carbon, volatile matter content, and dehydroxylation of mixture of the starting materials during sintering [29]. Another reason is the high porosity of zeolite and bentonite. The macropores on the surface of sintered filter have been observed. These can facilitate the flow of water [42]. EDS results revealed that the composition of filter obtained with sintering at 400 ºC is 29.07 wt.% C, 22.90 wt.% O, 18.15 wt.% Al, 22.42 wt.% Si, 2.12 wt.% Na, 0.63 wt.% Mg, 1.45 wt.% K 0.57 wt.% Ca, 1.59 wt.% Fe, and 1.07 wt.% B. These results showed a high concentration of carbon in the sintered filter, which is comparable to the carbon content in zeolite/activated carbon composites produced with calcination at 450 ºC and activation at 850 ºC [13]. The sintered filter is also abundant in O, Al, and Si, which correlates well with the XRD results. It was showed that the all of the elements are present in the form of oxides [43].

4. Conclusions: Sintered filters were prepared from mixtures of lignite, zeolite, bentonite, and clay. These filters are functionalizated and have a high content of aluminosilicates and carbon. The firing shrinkage, the total shrinkage, and hardness of sintered filters increased with increasing sintering temperature from 400 ºC to 600 ºC. The hardness of sintered filters is more than 700±10 *k*Pa or 7.1380 kg/cm^2. The porosity of the sintered filter is higher than that of the starting material lignite. The sintered filter made from mixture containing 45 wt.% lignite, 30 wt.% zeolite, 10 wt.% bentonite, 10 wt.% local clay, and 5 wt.% borax and sintered 400 ºC has potential to be used for heavy metal removal from aqueous solutions via cation exchange and adsorption processes.

Acknowledgement: The authors would like to thank the Chemistry Department, Faculty of Science, Naresuan University for the support of this project.

References:

[1] G. L. Athens, R. M. Shayib, B. F. Chmelka, Curr. Opin. Colloid Interf. Sci. 14 (2009) 281.
[2] A. C. Lopes, P. Martins, S. Lanceros-Mendez, Prog. Surf. Sci. 89 (2004) 239.
[3] M. Ahmaruzzaman, Adv. Colloid. Interfac. Sci. 143 (2008) 48.

[4] J. M. Gatica, H. Vidal, J. Hazard. Mater. 181 (2010) 18.
[5] S. Wang, Z. H. Zhu, J. Hazard. Mater. B136 (2006) 946.
[6] P. R. Shukla, S. Wang, H. M. Ang, M. O. Tadé, Adv. Powder Technol. 20 (2009) 245.
[7] C. Vohla, M. Koiv, H. J. Bavor, F. Chazarenc, U. Mander, Ecol. Eng. 37 (2011) 70.
[8] S. M. Lee, Lalhmunsiama, Thanhmingliana, D. Tiwari, Chem. Eng. J. 270 (2015) 496.
[9] H. Hadjar, B. Hamdi, C. O. Ania, J. Hazard. Mater. 188 (2011) 304.
[10] P. Anadão, I. L. R. Pajolli, E. A. Hildebrando, H. Wiebeck, Adv. Powder Technol. 25 (2014) 926.
[11] A. A. Halim, H. A. Aziz, M. A. M. Johari, K. S. Ariffin Desalination 262 (2010) 31.
[12] M. Ogura, Y. Zhang, S. P. Elangovan, T. Okubo, Micropor. Mesopor. Mat. 101 (2007) 224.
[13] Z. Li, X. Cui, J. Ma, W. Chen, W. Gao, R. Li, Mater. Chem. Phys. 147 (2014) 1003.
[14] M. J. Valero-Romero, E. M. Márquez-Franco, J. Bedia, J. Rodríguez-Mirasol, T. Cordero, Micropor. Mesopor. Mat. 196 (2014) 68.
[15] M. Miyake, Y. Kimura, T. Ohashi, M. Matsuda, Micropor. Mesopor. Mat. 112 (2008) 170.
[16] M. Karnib, A. Kabbani, H. Holail, Z. Olama, Energ. Procedia. 50 (2014) 113.
[17] C. Y. Tso, C. Y. H. Chao, Int. J. Refrig. 35 (2012) 1626.
[18] R. -L. Tseng, F. -C. Wu, R. -S. Juang, Sep. Purif. Technol. 140 (2015) 53.
[19] M. Houari, B. Hamdi, O. Bouras, J. -C. Bollinger, M. Baudu, Chem. Eng. J. 255 (2014) 506.
[20] C. de Sa, F. Benboudjema, M. Thiery, J. Sicard, Cement Concrete Comp. 30 (2008) 947.
[21] S. T. Rasmussen, W. Ngaji-Okumu, K. Boenke, W. J. O'Brien, Dental Materials 13 (1997) 43.
[22] F. Slaty, H. Khoury, J. Wastiels, H. Rahier, Appl. Clay Sci. 75–76 (2013) 120.
[23] S. Boycheva, D. Zgureva, V. Vassilev, Fuel 108 (2013) 639.
[24] A. Salem, R. A. Sene, Chem. Eng. J. 174 (2011) 619.
[25] L. Jie, D. Mei-fang, Y. Bo, Z. Zhong-xiao, J. Fuel Chem. Technol. 36 (2008) 519.
[26] A. Salem, S. Aghahosseini, Thermochim. Acta. 545 (2012) 57.
[27] X. Liu, F. Gao, C. Tian, J. Alloy. Compd. 486 (2009) 743.
[28] S. Mopoung, L. Anuwetch, S. Inkum, NU. J. 16 (2008) 127.
[29] T. P. Hoepfner, E. D. Case, Ceram. Int. 29 (2003) 699.
[30] Ch. Guiderdoni, C. Estournès, A. Peigney, A. Weibel, V. Turq, Ch. Laurent, Carbon. 49 (2011) 4535.
[31] J. Rizhikovs, J. Zandersons, S. Spince, G. Dobele, E. Jakab, J. Anal. Appl. Pyrol. 93 (2012) 68.
[32] T. A. M. Msagati, B. B. Mamba, V. Sivasankar, K. Omine, Appl. Surf. Sci. 301 (2014) 235.
[33] Y. Zhao, J. Zhang, C. Zheng, Int. J. Coal Geol. 94 (2012) 182.
[34] L. Hongqiang, F. Qiming, O. Leming, L. Sisi, C. Mengmeng, W. Xiaoqing, Int. J. Mining Sci. Technol. 23 (2013) 855.
[35] E. H. Park, U. S. Jeong, U. H. Jung, S. H. Kim, J. Lee, S. W. Nam, T. H. Lim, Y. J. Park, Y. H. Yu, Int. J. Hydrogen Ener. 32 (2007) 2982.
[36] M. J. Shen, X. J. Wang, M. F. Zhang, Appl. Surf. Sci. 259 (2012) 362.
[37] A. G. San Cristóbal, R. Castelló, M. A. M. Luengo, C. Vizcayno, Appl. Clay Sci. 49 (2010) 239.
[38] Z. -S. Liu, Y. -H. Peng, C. -Y. Huang, M. -J. Hung, Thermochim. Acta. 602 (2015) 8.
[39] O. Gezici, I. Demir, A. Demircan, N. Ünlü, M. Karaarslan, Spectrochim. Acta A. 96 (2012) 63.
[40] N. M. Musyoka, R. Missengue, M. Kusisakana, L. F. Petrik, Appl. Clay Sci. 97–98 (2014) 182.
[41] B. Weiwei, L. Lu, Z. Haifeng, G. Shucai, X. Xuechun, J. Guijuan, G. Guimei, Z. Keyan, Chinese J. Chem. Eng. 21 (2013) 974.
[42] K. B. Thapa, Y. Qi, S. A. Clayton, A. F. A. Hoadley, Water Res. 43 (2009) 623.
[43] G. Tozsin, Int. J. Coal Geol. 131 (2014) 1.